HHS Public Access

Author manuscript

ACS Biomater Sci Eng. Author manuscript; available in PMC 2016 November 09.

Published in final edited form as:

ACS Biomater Sci Eng. 2016 April 11; 2(4): 634–642. doi:10.1021/acsbiomaterials.6b00035.

In Vitro Cytotoxicity, Adhesion, and Proliferation of Human Vascular Cells Exposed to Zinc

Emily R. Shearier[†], **Patrick K. Bowen**[‡], **Weilue He**[†], **Adam Drelich**[‡], **Jaroslaw Drelich**[‡], **Jeremy Goldman**[†,*], and **Feng Zhao**[†,*]

[†]Department of Biomedical Engineering, Michigan Technological University, Houghton, Michigan, United States

[‡]Department of Materials Science and Engineering, Michigan Technological University, Houghton, Michigan, United States

Abstract

Zinc (Zn) and its alloys have recently been introduced as a new class of biodegradable metals with potential application in biodegradable vascular stents. Although an in vivo feasibility study pointed to outstanding biocompatibility of Zn-based implants in vascular environments, a thorough understanding of how Zn and Zn^{2+} affect surrounding cells is lacking. In this comparative study, three vascular cell types—human endothelial cells (HAEC), human aortic smooth muscle cells (AoSMC), and human dermal fibroblasts (hDF)—were studied to advance the understanding of Zn/Zn^{2+}-cell interactions. Aqueous cytotoxicity using a Zn^{2+} insult assay resulted in LD_{50} values of 50 μM for hDF, 70 μM for AoSMC, and 265 μM for HAEC. Direct cell contact with the metallic Zn surface resulted initially in cell attachment, but was quickly followed by cell death. After modification of the Zn surface using a layer of gelatin—intended to mimic a protein layer seen in vivo—the cells were able to attach and proliferate on the Zn surface. Further experiments demonstrated a Zn dose-dependent effect on cell spreading and migration, suggesting that both adhesion and cell mobility may be hindered by free Zn^{2+}.

Graphical Abstract

[*]**Corresponding Authors**. fengzhao@mtu.edu. Phone: 906-4872852. jgoldman@mtu.edu. Phone: 906-4872851. Address: 1400 Townsend Dr., 309 Minerals & Materials Bldg., Houghton, MI 49931.

ASSOCIATED CONTENT

Supporting Information

The Supporting Information is available free of charge on the ACS Publications website at DOI: 10.1021/acsbiomaterials.6b00035.

Materials and Methods; Figure S1, eosin stain of gelatin placed on glass and Zn surfaces; Figure S2, SEM images of protein layer present on Zn wire after direct blood exposure (PDF)

The authors declare no competing financial interest.

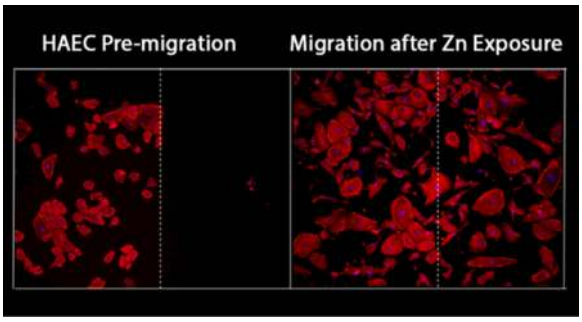

Keywords

zinc; stents; in vitro testing; cytotoxicity; biocompatibility

1. INTRODUCTION

Endovascular stent research in the last several years has focused on the development of bioabsorbable materials[1] of both polymeric[2,3] and metallic[4–7] composition. Within the metallic category, iron,[8,9] magnesium,[10–13] and zinc[14] have all been considered and investigated for this application. All three metals, however, have deficiencies vis-à-vis mechanical properties, biodegradation rate, or biodegradation product characteristics. Iron was one of the first metallic candidates for biodegradable stenting and has undergone considerable alloying development to control its mechanical properties and biodegradation rate.[15] Iron–manganese alloys[9,16] were among the most prominent candidates for endovascular stent applications. Although cytotoxicity[9] and in vivo studies[8] appeared to confirm the safety of iron implants, new studies with pure iron showed formation of a voluminous, biostable corrosion product during degradation in the abdominal aortas of rats.[17] The formation of biostable "rust" spurred the authors to cease development of iron-based bioabsorbable stents. Research on magnesium and its alloys, meanwhile, has yielded many new alloys,[18,19] new coating technologies,[20] detailed corrosion mechanisms,[21] refined benchtop corrosion methods,[22] and detailed information on biocorrosion kinetics.[23–25] Even with these substantial advances in bioabsorbable magnesium technology, an alloy has not yet been developed that is generally regarded as simultaneously possessing mechanical properties, corrosion resistance, and arterial biocompatibility sufficient for stent application.[26,27]

Zinc (Zn) and its alloys have been studied over the last 4–5 years as an alternative base material to iron and magnesium.[14] Pure Zn possesses an intrinsically low corrosion rate[14] – under the proposed 20 μm/year limit[28] – and does not visibly affect the adjacent tissue.[39] Other recent experimental work by Vojtzěch et al.[29,30] on Zn and its alloys for orthopedic application noted a general lack of toxicity data for metallic Zn. The recommended daily value (RDV) for Zn as a micronutrient[31] may be a useful guideline for estimating the potential for gross systemic toxicity. Some case studies and general references discuss systemic toxicity responses stemming from chronic or acute Zn ingestion,[32–36] but these reports are fairly sparse. This does indicate that orthopedic implants[29,37] made of Zn and its alloys should be approached with caution because of their relatively large masses and

surface areas. In contrast, systemic Zn toxicity appears to be highly unlikely in the case of small Zn-based implants such as stents, sutures, staples, or vascular clips. First-approximation Zn^{2+} release rates from a stent comprising 50 mg of pure Zn were previously estimated to be about 150 μg/day, well below the corresponding RDV for all age groups.[14]

Although the RDV and the potential for gross systemic toxicity are important considerations, local material biocompatibility should also be fully considered. Performance of the implant is dictated by the microenvironment in which the material is placed, as well as the nature of the biological milieu.[38] A few studies have examined in vitro cytotoxicity of ionic Zn^{2+}. Schaffer et al.[39] reported a relatively high Zn^{2+} tolerance for human aortic cell types; endothelial and smooth muscle cells were reported to exhibit 50% survival at Zn^{2+} concentrations of 340 and 330 μM, respectively. However, this value exceeds the total Zn^{2+} content of a human HT-29 (immortalized colon cancer) cell line by ~50% according to Krezel and Maret;[40] it exceeds the determined free Zn^{2+} buffering capacity for the same cells (ca. 28 μM) by an order of magnitude. The reason for this large discrepancy is not clear. Murni et al.[37] performed a cytotoxicity evaluation on Zn-3 wt % Mg using the extract method on primary human osteoblasts. When the osteoblasts were exposed to Zn–containing extracts with Zn^{2+} concentrations of approximately 0.5 ppm (~8 μM), their viability was reduced to 30–50% of the control. Using the same insult method, Murni et al.[37] found that common inflammatory markers (interleukin 1-beta, cyclooxygenase-2, and prostaglandin E_2) were not expressed in significant quantities after in vitro exposure to Zn^{2+}. This indicated that Zn^{2+} is not proinflammatory, per se, though the relative lack of cell signaling in vitro may require re-examination of this issue with in vivo methods. Recently, in a study done by Ma et al.[41] on ionic zinc's (Zn^{2+}) effect on coronary artery endothelial cells (HCECs), authors were able to show a biphasic change in cell viability, with increased cell viability at 20 μM and inhibited cell viability at 100 μM. The endothelial cells' spreading and migration was also investigated, and showed a similar trend to viability: low Zn^{2+} concentrations enhanced and higher Zn^{2+} concentrations inhibited the HCECs' spreading and migration, respectively.

A recent histological (in vivo) study by the authors[42] examined pure (99.99%) Zn wires that were implanted in a transluminal fashion in the abdominal aortas of rats, with a large portion of the wire positioned along the endothelium and exposed to blood flow. That study concluded that pure, metallic Zn and its corrosion products were noninflammatory, antiproliferative toward smooth muscle cells, possibly antirestenotic, and did not foster any necrosis or other local toxicity. This experience provides an in vivo benchmark for subsequent in vitro evaluations of Zn-based cardiovascular biomaterials. An appropriate in vitro test conducted on the same material should therefore produce results in agreement with the in vivo benchmark for vascular cells.

In this study, aqueous insult of Zn^{2+} was carried out with primary human vascular cell types in an attempt to explain in vivo results published in[42] and establish a valid approach toward toxicity investigation of this material family. Zn direct contact cell culture was also performed on both bare metal and gelatin-modified surfaces. Finally, the effect of Zn^{2+} on cell size, spreading, and migration was investigated.

2. METHODS AND MATERIALS

2.1. Materials and Reagents

Reagent-grade sodium chloride, potassium chloride, calcium chloride, magnesium chloride hexahydrate, zinc chloride, sodium hydroxide, Type B bovine skin gelatin with a bloom of ~225 g, hexamethyldisilazane (HMDS), Tris-(hydroxymethyl)aminomethane hydrochloride (TRIS-HCL), dopamine hydrochloride, N-(3-(Dimethylamino)propyl)-N′-ethylcarbodiimide hydrochloride (EDC), formalin solution-10%, 2-(*N*-morpholino) ethanesulfonic acid hydrate (MES), fibronectin, and human plasma were obtained from Sigma-Aldrich (St. Louis, MO). Zn foils of 99.9%+ purity were obtained from ThyssenKrupp Materials via OnlineMetals.com (Seattle, WA) in foil form, with a nominal thickness of 500 μm and precut to a size of 12.5 × 12.5 mm using hydraulic shearing. This purity was chosen due to the availability in foil form. Acetone (HPLC-grade, 99%), absolute ethanol, and isopropanol (99%) were obtained from Pharmco-Aaper (Brookfield, CT). The tetrazolium salt assay kit based on 2,3-bis(2-methoxy-4-nitro-5-sulfophenyl)-2H-tetrazolium-5-carboxanilide (XTT) was purchased from ATCC (Manassas, VA). FDA grade silicone rubber, 40A durometer, was purchased from McMaster (Elmhurst, IL). Nuclear fluorescent staining was achieved using 4′,6-diamidino-2-phenylindole (DAPI) from Life Technologies (Carlsbad, CA). F-actin was visualized using Phallodin obtained from Abcam (Cambridge, MA). Live/dead staining was performed using a live/dead cell staining kit containing propidium iodide and calcein, also purchased from Abcam.

2.2. Cells and Culture

The cell types used in these cytotoxicity tests included human dermal fibroblasts (hDF) to represent adventitial tissue, human aortic smooth muscle cells (AoSMC) to mimic the tunica media, and human aortic endothelial cells (HAEC) as a stand-in for the tunica intima. The hDF were acquired from ATCC and cultured in Dulbecco's Modified Eagle Media (DMEM) supplemented with 20% fetal bovine serum (FBS), 20% Ham F12, 500 μM sodium ascorbate, and 1% penicillin/streptomycin (Life Technologies) at passage 3–8. AoSMC were purchased from Lonza (Walkersville, MD) and cultured in Smooth Muscle Growth Media BulletKit (Lonza) at passage 3–5. HAEC were also bought from Lonza, and were cultured using Endothelial Cell Growth Media BulletKit at passage 3–5. Cellstar pretreated culture dishes were purchased from Sigma-Aldrich, and all culture was carried out in a VWR Symphony incubator (Radnor, PA) at 37 °C and 5% CO_2.

2.3. Zn^{2+} Insult and XTT Assay

Zn salt ($ZnCl_2$) was observed to be incompatible with culture media, as the buffering environment caused the immediate precipitation of $ZnO/Zn(OH)_2$ on addition of the salt. Therefore, a pseudophysiological chloride solution buffered with MES was designed to carry the Zn^{2+} without precipitation of zinc oxide, zinc hydroxide, and zinc salts, as well as to limit the intrinsic Zn^{2+} buffering capacity of the insult solution (e.g., by removing Zn^{2+}-albumin interactions). The base chloride solution consisted of 131 mM NaCl, 4 mM KCl, 2.5 mM $CaCl_2$, and 1 mM $MgCl_2$ in deionized H_2O to mimic the composition of human whole blood.[43] Twenty mM MES was added to the solution, and the solution's pH was fixed at 6.00 ± 0.02 via incremental additions of 1 M NaOH. At a pH of ~6, the Pourbaix diagram

indicated that Zn^{2+} would remain stable in solution to very high concentrations, as seen in Figure 1.[44] A 1 mM $ZnCl_2$ solution was prepared through serial dilution of 10 M $ZnCl_2$ with the pseudophysiological chloride solution. A series of 18 dilute $ZnCl_2$ insult solutions was prepared with compositions ranging from 1 to 500 μM, with Zn^{2+} concentrations uniformly distributed in $\log_{10}$ space. The real level of Zn^{2+} in the solutions was determined by inductively coupled plasma optical emission spectroscopy (ICP-OES) using a PerkinElmer 7000DV (Waltham, MA). The ICP-OES detection limit for Zn^{2+} was 6 ppb.

Cells were seeded at a level of 5000 cells/cm^2 into 96-well plates and cultured in their respective media for 48 h. The media was then aspirated, wells rinsed with phosphate-buffered saline to remove any residual buffering agent, and the pseudophysiological chloride solution doped with $ZnCl_2$ was added after filtering through a 0.22 μm membrane. The same solution with no Zn^{2+} was used as a control. Eight replicates were used at each insult level for all cell types. The insult period was fixed at 4 h; longer times were avoided to prevent major phenotypical changes in the cells due to starvation. The insult solution was aspirated, cells rinsed with culture media, and fresh media added before the cells were allowed to recover for 24 h. This allowed time for resolution of any apoptotic or latent necrotic cell death pathways.

After the recovery period, a XTT assay was performed to measure the activity of cellular enzymes and quantify relative number of viable cells present in the sample. Calibration and execution of the assay followed the manufacturer's recommendations/instructions. Color intensities for blank, control, and experimental samples were recorded using a VERSA Max Tunable microplate reader (Molecular Devices; Silicon Valley, CA). After processing, the cell viabilities in the experimental group were reported as a percentage of the control sample.

2.4. Direct Culture on Metallic Zn

Zn foils were degreased by ultrasonic cleaning in acetone with a 40 kHz/230 W Branson Ultrasonics 2510 unit (Danbury, CT) for 5 min. The acetone was decanted and replaced with isopropanol, after which the foils were ultrasonically cleaned for another 5 min. The foils were stored under isopropanol until they were air-dried in the sterile culture hood. The Zn foils were placed on the bottom of 24-well plates, and cells were seeded on top at a cell density of 5×10^3 cells/cm^2. Glass coverslips were used as a cytocompatbile control material. Incubation times ranged from 2 h (initial attachment) up to 96 h. The specimens were then processed for either fluorescent microscopic examination (Section 2.7) or analysis via scanning electron microscopy (Section 2.8).

2.5. Modification of the Zn Surface

The surface of the metallic Zn was modified by attaching a gelatin sheet of controlled thickness. An intermediate layer of dopamine was first applied to the Zn surface, and used to covalently bond with the gelatin, thereby ensuring the gelatin remained anchored under cell culture conditions. A solution of 7.7 mM Tris-HCl was prepared with double-distilled H_2O and adjusted to a pH of 8.5. Two mg/mL of dopamine hydrochloride was dissolved in the TRIS solution. Zn foils were incubated in the dopamine solution under culture conditions for

12 h, after which a darkening of the dopamine-Tris solution was observed, confirming that dopamine polymerization had occurred. The foils were removed and rinsed with double-distilled H_2O.

Gelatin was used in able to create stable cylinders that could be sectioned into layers of highly controlled thickness. This allowed reproducible results, while creating a barrier between the cells and the Zn foils. A 50 mg/mL bulk collagen gel was created by dissolving 0.5 g bovine skin gelatin in 10 mL of deionized H_2O heated to ~70 °C, stirring to generate a small vortex. While still hot, the solution was poured into a 15 mL culture tube (12.5 mm inner diameter) and allowed to gel overnight at 4 °C. The gelatin and tube were then cut into cylindrical segments measuring 15–20 mm in length with a razor blade, wrapped in at least two layers of Parafilm, and snap-frozen in liquid nitrogen. The Parafilm was then removed, and the frozen tube and gelatin were briefly rolled on the surface of a warm hot plate until the interface loosened just slightly, and allowed the frozen gelatin to be pushed out of the plastic tube. The gelatin cylinders were stored at −80 °C prior to mounting and sectioning.

A Microm HM 550 P histological cryomicrotome (Waldorf, Germany) was used to prepare gelatin sheets of uniform thickness. The gelatin cylinders were affixed to aluminum sample mounts using PolyFreeze (Polysciences, Inc.; Warrington, PA) set at −40 °C for several minutes. The sample assembly was then relocated to the sectioning arm and allowed to gradually warm to −10 °C. When the gelatin was sectioned at a lower temperature, the gel tended to form discontinuous “shavings” or fracture outright. Once warmed, the frozen gelatin was trimmed to yield a planar surface. A 100 μm–thickness section was produced, and affixed to the warm, dopamine-coated Zn foil simply by bringing them into contact. Gelatin-covered foils were then immersed in 10 mM EDC in 90% ethanol for 20 min to cross-link the gelatin, thereby preventing dissolution in the culture medium and simultaneously sterilizing the samples. The foils were then rinsed with PBS and full culture media to remove any traces of the cytotoxic EDC. Verification of gelatin coating, both immediately after placement and 24 h after incubated in PBS, was performed (see Supporting Information).

The three cell types (AoSMC, HAEC, and hDF) were then seeded on the gelatin-covered foils at a density of 5×10^3 cells/cm^2. Culture times ranged from 2 to 24 h, with live/dead staining immediately following harvest, or immersion in 10% (w/v) formalin at 4 °C for 48 h for fluorescent microscopy. Resulting specimens were analyzed with fluorescent microscopic techniques, described in Section 2.7.

2.6. Fibronectin Coating and Migration Assay

Purchased human plasma fibronectin was reconstituted at a concentration of 1 mg/mL. Glass coverslips and Zn foils were sterilized via 70% ethanol and UV light. Fibronectin stock solution was then diluted using PBS to 3 μg/cm^2 with minimal volume added to the surfaces. This was then allowed to air-dry for 45 min at room temperature. Cells were seeded at a density of 5×10^3 cells/cm^2 and allowed to grow for 24 h. These samples were then exposed to media containing Zn in levels varying from 1 to 200 μM for 24 h. Live/dead and fluorescent imaging was then performed as described in Section 2.7.

For migration experiments, the surfaces were also treated with fibronectin as described above. A square silicone mask with a rectangle punched from the center was used to restrict the area of initial cell attachment. The inner rectangle had dimensions of 4.50 ± 0.10 × 12.00 ± 0.15 mm, and the outer square was 15.15 ± 0.15 mm square. The thickness of the mask was 1.61 ± 0.02 mm. After fibronectin coating, the mask was placed over the square glass coverslips and cells were seeded on the top, ensuring that cell attachment occurred only within the punched-out rectangle. These cells were cultured for 24 h, the masks were removed, and the cells were then exposed to media containing Zn^{2+} in levels varying from 1 to 200 μM for 24 h. Fluorescent imaging and quantification was then performed as described in Section 2.7.

2.7. Fluorescent Imaging

Fluorescent staining was carried out on the samples after 48 h in 10% formalin. Samples were permeabilized using 0.2% (w/v) Triton-100 in PBS and blocked using a 1% (w/v) bovine serum albumin in PBS. F-actin was used to show filamentous proteins within the cytoplasm and was diluted at 1:100 in PBS. DAPI, used to visualize cell nuclei, was diluted at 1:1000 in PBS.

Live/dead staining was completed using a live/dead cell staining kit. Calcein and propidium iodide were both diluted at 1:1000 in staining buffer and introduced to cells growing directly on the surface of interest. This was incubated for 15 min at 37 °C before imaging. A viability ratio for the experimental groups of interest was calculated using control glass slides covered with the corresponding coating (for example, Zn coated with gelatin's viability ratio was calculated using a glass coverslip coated with gelatin as a control). Three samples were obtained for each, with three random areas of interest used on each sample.

Fluorescent imaging utilized an Olympus BX-51 fluorescent microscope (Olympus America; Center Valley, PA). Random fields of view were imaged and confirmed to be representative ex post.

Cell area was calculated using cells stain with F-actin and DAPI, with all cells measured. Distance migrated was determined via measurement of the distance from the nearest edge of the mask to the center of each cell. Total cells migrated out of this area was also calculated.

2.8. FE-SEM Examination

After removing from the culture conditions, cells on Zn foils were fixed with 10% formalin. Dehydration was done with a series of ethanol-deionized H_2O solutions (10, 30, 50, 70, 90, and 100 vol % absolute ethanol). After the last dehydration series step, the absolute ethanol was removed from the specimens and replaced with HMDS, which was allowed to evaporate fully in a chemical hood. The cells and foils were relocated to the low-humidity environment of a desiccator prior to platinum coating to improve surface conductivity. Samples were then imaged with a Hitachi S-4700 cold field emission scanning electron microscope (FE-SEM) (Hitachi High Technologies America; Pleasanton, CA) operated at 10 kV accelerating voltage and an emission current of 5–7 μA.

2.9. Statistical Methods

Quoted errors and error bars correspond to sample standard error. Beers' approach to the propagation of random errors[46] was used to calculate overall standard errors for XTT cell viability that took into account random error in measurements from the experimental group, control group, and background (blank) samples. ImageJ was used to measure cell area and cell migration.[45] Minitab was used for statistical analysis of the migration experiment.[47]

3. RESULTS

3.1. Zn^{2+} Insult and XTT Cell Viability Assay

Cell viability following Zn^{2+} insult, recovery, and analysis using the XTT assay are presented in Figure 2 with trend lines to guide the eye. The apparent median lethal dose (LD_{50}) values were 3.5 ppm (50 μM) for hDF, 4.5 ppm (70 μM) for AoSMC, and 17.5 ppm (265 μM) for HAEC.

The hDF and AoSMC viabilities tended to decrease similarly through the entire range of concentrations examined, with very few cells remaining at concentrations greater than ~10 ppm (~150 μM). HAEC exhibited superior tolerance for Zn^{2+} across a wide range of concentrations, as evidenced by the 4–5-fold higher LD_{50} in comparison to the other cell types.

3.2. Direct Culture on Metallic Zn

Because HAEC proved to be the most resilient cell type in the presence of ionic zinc, studies with direct culture concentrated on this cell type. A stark difference in apparent cell viability and morphology was observed between HAEC cultured on glass coverslips and those cultured on zinc foils (Figure 3). The cells in Figure 3 were stained for F-actin (red) and counterstained with DAPI to highlight the cell nuclei (blue). The control HAEC group–those cultured on glass coverslips–exhibited rapid attachment and spreading at 2 and 6 h (Figure 3A, B, respectively), with F-actin filaments readily extending to the glass substrate, anchoring the cells. After 96 h of culture on glass (Figure 3C), the cells were visible at a high density and had nearly achieved confluence. In addition, many of cells were observed to possess two nuclei, indicative of telophase mitosis. The healthy HAEC on glass are distinct from the F-actin/DAPI-stained Zn foil culture specimens at all of the time points (Figure 3B, D, F). Two hours after seeding (Figure 3B), few nuclei were visible. The few that did fluoresce appeared to be more-or-less spherical, as the F-actin signature was barely distinct from the DAPI signature. At 6 and 96 h (Figure 3D, F, respectively), no cells were readily identifiable. Instead, small, globular features surrounded by a halo measuring ca. 60–70 μm in diameter appeared to fluoresce. The sizes of these features were approximately the same as a single, healthy HAEC. Because Zn oxide and hydroxide are fluorescent minerals, it is not clear what, if any, of the fluorescent signal is actually indicative of DAPI binding.

The morphologies of HAEC and hDF were examined after a 24 h culture cycle using FE-SEM (Figure 4) as a complementary technique to immunofluorescence. HAEC seeded on glass (Figure 4A) and hDF seeded on glass (Figure 4C) were both healthy-looking, which cells exhibiting morphologies typical of endothelial cells and fibroblasts, respectively. In

contrast, the HAEC seeded directly on metallic Zn (Figure 4B) bore little resemblance to the cells on glass. Small, globular features surrounded by a round corrosion "halo" were distributed on the surface, and were presumably the remains of HAEC. The hDF (Figure 4D) responded differently to the Zn surface than the HAEC, in that they appeared mostly intact and anchored on the metallic surface. The membranes of most hDF visible on the Zn foil had been disrupted in some way. The cellular contents were often expelled and were seen surrounding the dead cell. These results were in agreement with the immunofluorescent evaluation. Cell survival on the Zn surface was negligible.

3.3. Cell Response to Modified Zn Surface

Because of the lack of viability when culturing directly on the Zn surface, an experiment more representative of what cells will contact in vivo was desired. In a separate *in vivo* experiment (see Supporting Information), it was observed that after even a short contact time with blood, a stable, confluent protein layer is formed on Zn surface, with which circulating and migrating cells are in direct contact. To mimic this protein layer in vitro, a controlled 100 μm-thick section of collagen based gelatin was attached via polymerized dopamine interactions with the Zn surface. Cells were exposed to this surface for 2 and 24 h, with viability ratios determined using a live/dead fluorescent stain. Significantly higher viability ratios were observed in both the dopamine-coated Zn and the Zn coated with gelatin than on the Zn disc at 24 h, as shown in Figure 5. As is visible in the live/dead fluorescent images in Figure 5, the morphology of all three vascular cell types was affected and resulted in a more rounded phenotype when cultured on a modified Zn surface (bottom panel) compared to control surface (top panel).

This phenotype was further investigated via fluorescent staining of F-actin and DAPI, both at 2 and 24 h. Cells cultured on the modified Zn surface were imaged and cell area was quantified, as shown in Figure 6. Images used in Figure 6 were cropped areas of a nominal 200× magnification to increase depth of field. Cell area was significantly reduced in both AoSMC and hDF, but HAEC showed no change in cell area after 24h.

3.4. Migration of Cells under Influence of Ionic Zn

As described by results in Section 3.3, Zn^{2+} can induce a dose-dependent inhibition of cell viability, possibly due to integrin interactions. To investigate the potential effect of Zn^{2+} on vascular cell migration and spreading, we initially seeded cells within a silicone mask on a surface coated with fibronectin, exposed to sub-LD_{50} levels of Zn^{2+}, and allowed to migrate for 24 h. At high Zn^{2+} concentrations hDF and AoSMC were not analyzed due to toxicity. The initial seeding area is indicated in Figure 7 with a dashed white line. For all cell types, the number of cells that migrated out of the initial seeding area decreased as the level of Zn^{2+} increased. HAEC were least affected by the Zn^{2+} levels, with these cells exhibiting the largest distance traveled and a smaller decrease in the total number of cells migrating out of the initial attachment area.

4. DISCUSSION

4.1. Zn^{2+} Aqueous Cytotoxicity

We report here the reaction of vascular cells upon exposure to Zn—both ionic and solid—in vitro. The first, and most basic, cytotoxicity assay performed was an aqueous exposure to free (unbound) Zn^{2+} ions. The LD_{50} values found for the vascular cell types evaluated were 50 μM for hDF, 70 μM for AoSMC, and 265 μM for HAEC (Figure 2), which are roughly in the same range as values reported by Schaffer et al. (330–340 μM).[39] The reason for the lower LD_{50} values in this study could be due to the exposure system. In the supplemented media exposure system, free Zn^{2+} is available to bind to the protein components of the serum, therefore lowering the amount of free Zn^{2+} the cells are directly exposed to. The method developed in this study may therefore lead to more accurate LD_{50} measurements, and likely contributed to the relatively low uncertainty and small error relative to previous studies. This method is also far superior to simple extract tests, allowing for greater control of Zn exposure.[48] When looking specifically at endothelial cells, the Zn^{2+} level recently reported by Ma et al. that caused a "lowered viability" of the exposed cells was above 100 μM. This value was not an LD_{50}, but rather a data point where the viability was significantly reduced, in a statistical sense, from the control value. It should be noted that, even though "statistically significant reduction" was specified as a threshold criterion for toxicity, the propagation of random errors was neglected. It is thus difficult to compare the results of Ma et al. to this study's endothelial cell LD_{50} value of 265 μM.[41]

It is important to note the highest LD_{50} value, corresponding to the highest Zn^{2+} tolerance, was found for HAEC. This is of particular interest for endovascular stent application, as the endothelium is the first layer of cells coming into contact with the metallic stent during implantation.[49] They also play an important role shortly thereafter during re-endothelialization.[50] In contrast, AoSMC had a poor tolerance for Zn^{2+}. This finding may be of significance later in the healing process, where smooth muscle cells that assume a proliferative phenotype, contribute to neointimal hyperplasia and, if left unchecked, to in-stent restenosis.[51] It was noted previously[42] that the density of α actin-positive cells (presumably smooth muscle cells) was low near the metallic Zn-tissue interface. It is possible that the relative Zn^{2+} sensitivity of this cell type could account for the observed lack of smooth muscle cell proliferation following an acute arterial puncture injury with metallic Zn.

4.2. Zn Direct Contact

When the vascular cells used in this study were cultured directly on the metallic Zn surface, there was minimal viability (Figure 3). The cells attached to the Zn surface to an extent, but died within 2 h. As shown by SEM images in Figure 4, intact endothelial cells are almost completely absent, whereas the hDF appear to be lysed or burst, corresponding to a sudden mode of death. This could be explained by different routes of cell death, including apoptosis versus necrosis.[52] The relatively more controlled appearance of HAEC may indicate death via apoptosis, whereas hDF may undergo necrosis as evidenced by the morphology of the cellular remnants. The aqueous cytotoxicity responses of the two cell types may explain this

difference; HAEC have a higher tolerance for or ability to process Zn^{2+} than hDF, and so fibroblasts may be easily overwhelmed and die in a necrotic fashion when exposed to Zn^{2+}.

When discussing the general lack of viability in the direct in vitro cell culture, the primary explanation for this is the lack of a confluent protein layer. The authors have previously observed the formation of a stable biological layer on Zn wires exposed to flowing blood within 24 h, which appeared to be approximately 100 μm thick (Supporting Information). Because this layer is formed so quickly in vivo, it is acceptable to assume that cells participating in reendothelialization of a Zn stent would not directly interact with the metallic Zn, but rather with this acquired protein coating. Following modification of the Zn surface using a layer of gelatin 100 μm thick, all three cells types were able to attach and replicate on the Zn surface (Figures 4 and 5), albeit at a slower rate and with a more rounded phenotype than on the control (glass coated with gelatin) surfaces. It is important to note the cells' viability ratios on dopamine coated surfaces were comparable to gelatin coated at lower time points. This could indicate the surface modifications not only act as an intermediate layer between the cells and the Zn surface, but also as an intermediate that enhances cell initial attachment.

Another consideration is that static in vitro culture cannot replicate the dynamic environment the cells experience in vivo with respect to both biochemistry and fluid flow. It is therefore possible that an increased local concentration of Zn^{2+} released from the metallic Zn surface is experienced by the cells in the absence of fluid flow past the metallic material. This could be confirmed in future work using, for example, an ion probe in static and flowing environments in vitro, but was beyond the scope of this contribution. In addition to fluid flow considerations, in vivo Zn^{2+} binding/sequestration and removal mechanisms exist, not only in flowing blood, but also within the arterial wall and interstitial fluid due to specific proteins (e.g., metallothioneins) which possess a high affinity for free Zn^{2+}.[53]

4.3. Cell morphology, spreading, and migration in response to Zn^{2+}

After observing the rounded phenotypes of cells on the coated Zn surface (Figure 5), an explanation for this phenomenon was explored. It is known that divalent cations interact with integrins, which are a family of adhesion metallo-protein receptors.[54–57] These proteins are highly regulated by divalent cations, with several studies showing specifically how Zn^{2+} induces a dose-dependent inhibition of cell adhesion and migration.[58–62] Unfortunately, none of these studies used vascular cell types similar to this contribution, and thus cannot be applied directly to the behavior of cells adjacent to a degradable endovascular stent. Specific integrins found to become affected by Zn^{2+} in these previous studies were those that interacted strongly with the extracellular matrix protein fibronectin. Therefore, migration experiments were performed on a surface coated with this molecule of interest.[58,59]

First, cell size was quantified to compare 2 and 24 h to determine if cell spreading was affected by Zn^{2+} (Figure 6). Both hDF and AoSMC experienced a reduction in cell size, whereas HAEC were unaffected. Migration experiments yielded similar results (Figure 7): all cell types experienced a decrease in migration with increasing Zn concentration. Again, the effect on HAEC was the weakest of all cell types evaluated. It appears that the spreading and migration of hDF and AoSMC are drastically affected by increasing Zn^{2+}

concentrations. HAEC spreading and migration is also inhibited at high Zn^{2+} concentrations, but to a lesser extent than hDF or AoSMC. This could be due at least partially to integrin interaction, but would require future experiments to verify which integrins are affected. Alternatively, it is also possible that this reaction could be due to another protein that is regulated by Zn^{2+}. It is well-known that Zn^{2+} participates in a multitude of protein structures throughout the cell, and, therefore, it would be useful to perform an in-depth in vitro investigation of protein regulation by Zn^{2+} in vascular cells in the future.

5. CONCLUSIONS

In this study, an in depth, comparative in vitro cytotoxicity analysis using vascular cell types was performed on Zn for use in biodegradable stents. Aqueous cytotoxicity showed LD_{50} values were 3.5 ppm (50 μM) for hDF, 4.5 ppm (70 μM) for AoSMC, and 17.5 ppm (265 μM) for HAEC. Of the three vascular cell types, HAEC appear to have the highest tolerance for Zn. All three cell types were able to attach and proliferate on a modified Zn surface, reflecting what has been observed in vivo. Cell area was significantly reduced over time for both hDF and AoSMC on modified Zn surface. For all three cell types the number of cells migrating out of original seeding area decreased with increasing Zn^{2+} concentration. Because of these results, it was concluded that cell attachment, spreading, and migration was affected by increased levels of Zn, particularly in the hDF and AoSMC.

Supplementary Material

Refer to Web version on PubMed Central for supplementary material.

Acknowledgments

U.S. National Institutes of Health, National Institute of Biomedical Imaging and Bioengineering (Grant 5R21 EB 019118-02 to J.D.), and National Heart, Lung, and Blood Institute (Grant 1R15HL115521-01A1 to F.Z., Grant 1R15HL129199-01 to J.G.), as well as Michigan Technological University (Research Excellence Fund-Research Seed Grant (REF-RS) to F.Z.) are acknowledged for funding this work. P.K.B. was supported by an American Heart Association predoctoral research fellowship administered by the Midwest Division. Mick Small and Jessica Walitalo from the Applied Chemical and Morphological Analysis Laboratory at Michigan Tech are gratefully acknowledged for their help with conductive coating of FE-SEM specimens. Jennifer Eikenberry is acknowledged for her assistance with ICP-OES analysis, and Roger Guillory II is gratefully acknowledged for his help with cryomicrotome sectioning.

REFERENCES

1. Mani G, Feldman MD, Patel D, Agrawal CM. Coronary stents: a materials perspective. Biomaterials. 2007; 28:1689–1710. [PubMed: 17188349]
2. Onuma Y, Ormiston J, Serruys PW. Bioresorbable scaffold technologies. Circ. J. 2011; 75:509–520. [PubMed: 21301138]
3. Campos CAM, Zhang Y-J, Bourantas CV, Muramatsu T, Garcia-Garcia HM, Lemos PA, et al. Bioresorbable vascular scaffolds in the clinical setting. Interv Cardiol. 2013; 5:639–646.
4. Hermawan H, Dube D, Mantovani D. Developments in metallic biodegradable stents. Acta Biomater. 2010; 6:1693–1697. [PubMed: 19815097]
5. Waksman R, Pakala R. Biodegradable and bioabsorbable stents. Curr. Pharm. Des. 2010; 16:4041–4051. [PubMed: 21208182]
6. Moravej M, Mantovani D. Biodegradable metals for cardiovascular stent application: interests and new opportunities. Int. J. Mol. Sci. 2011; 12:4250–4270. [PubMed: 21845076]

7. Patel N, Banning AP. Bioabsorbable scaffolds for the treatment of obstructive coronary artery disease: the next revolution in coronary intervention? Heart. 2013; 99:1236–1243. [PubMed: 23474621]
8. Peuster M, Hesse C, Schloo T, Fink C, Beerbaum P, von Schnakenburg C. Long-term biocompatibility of a corrodible peripheral iron stent in the porcine descending aorta. Biomaterials. 2006; 27:4955–4962. [PubMed: 16765434]
9. Hermawan H, Purnama A, Dube D, Couet J, Mantovani D. Fe-Mn alloys for metallic biodegradable stents: degradation and cell viability studies. Acta Biomater. 2010; 6:1852–1860. [PubMed: 19941977]
10. Heublein B, Rohde R, Kaese V, Niemeyer M, Hartung W, Haverich A. Biocorrosion of magnesium alloys: a new principle in cardiovascular implant technology? Heart. 2003; 89:651–656. [PubMed: 12748224]
11. Di Mario C, Griffiths H, Goktekin O, Peeters N, Verbist J, Bosiers M, et al. Drug-eluting bioabsorbable magnesium stent. J. Interv Cardiol. 2004; 17:391–395. [PubMed: 15546291]
12. Schranz D, Zartner P, Michel-Behnke I, Akinturk H. Bioabsorbable metal stents for percutaneous treatment of critical recoarctation of the aorta in a newborn. Catheter Cardiovasc Interv. 2006; 67:671–673. [PubMed: 16575923]
13. Waksman R, Pakala R, Kuchulakanti PK, Baffour R, Hellinga D, Seabron R, et al. Safety and efficacy of bioabsorbable magnesium alloy stents in porcine coronary arteries. Catheter Cardiovasc Interv. 2006; 68:607–617. discussion 18–19. [PubMed: 16969879]
14. Bowen PK, Drelich J, Goldman J. Zinc exhibits ideal physiological corrosion behavior for bioabsorbable stents. Adv. Mater. 2013; 25:2577–2582. [PubMed: 23495090]
15. Liu B, Zheng YF. Effects of alloying elements (Mn, Co, Al, W, Sn, B, C, and S) on biodegradability and in vitro biocompatibility of pure iron. Acta Biomater. 2011; 7:1407–1420. [PubMed: 21056126]
16. Hermawan H, Alamdari H, Mantovani D, Dubé D. Iron–manganese: new class of metallic degradable biomaterials prepared by powder metallurgy. Powder Metall. 2008; 51:38–45.
17. Pierson D, Edick J, Tauscher A, Pokorney E, Bowen PK, Gelbaugh J, et al. A simplified in vivo approach for evaluating the bioabsorbable behavior of candidate stent materials. J. Biomed. Mater. Res., Part B. 2012; 100B:58–67.
18. Seitz JM, Eifler R, Stahl J, Kietzmann M, Bach FW. Characterization of MgNd2 alloy for potential applications in bioresorbable implantable devices. Acta Biomater. 2012; 8:3852–3864. [PubMed: 22676917]
19. Li N, Zheng Y. Novel magnesium alloys developed for biomedical application: A review. J. Mater. Sci. Technol. 2013; 29:489–502.
20. Hornberger H, Virtanen S, Boccaccini AR. Biomedical coatings on magnesium alloys–a review. Acta Biomater. 2012; 8:2442–2455. [PubMed: 22510401]
21. Bowen PK, Drelich J, Goldman J. Magnesium in the murine artery: Probing the products of corrosion. Acta Biomater. 2014; 10:1475–1483. [PubMed: 24296127]
22. Kirkland NT, Birbilis N, Staiger MP. Assessing the corrosion of biodegradable magnesium implants: a critical review of current methodologies and their limitations. Acta Biomater. 2012; 8:925–936. [PubMed: 22134164]
23. Kirkland NT, Lespagnol J, Birbilis N, Staiger MP. A survey of bio-corrosion rates of magnesium alloys. Corros. Sci. 2010; 52:287–291.
24. Bowen PK, Drelich J, Goldman J. A new in vitro-in vivo correlation for bioabsorbable magnesium stents from mechanical behavior. Mater. Sci. Eng., C. 2013; 33:5064–5070.
25. Bowen PK, Drelich A, Drelich J, Goldman J. Rates of in vivo (arterial) and in vitro biocorrosion for pure magnesium. J. Biomed. Mater. Res., Part A. 2015; 103:341–349.
26. Haude M, Erbel R, Erne P, Verheye S, Degen H, Bose D, et al. Safety and performance of the drug-eluting absorbable metal scaffold (DREAMS) in patients with de-novo coronary lesions: 12 month results of the prospective, multicentre, first-in-man BIO-SOLVE-I trial. Lancet. 2013; 381:836–844. [PubMed: 23332165]
27. Li H, Zheng Y, Qin L. Progress of biodegradable metals. Prog. Nat. Sci. 2014; 24:414–422.

28. Werkhoven, RJ.; Sillekens, WH.; van Lieshout, JBJM. Processing aspects of magnesium alloy stent tube. In: Sillekens, WH.; Agnew, SR.; Neelameggham, NR.; Mathaudhu, SN., editors. Magnesium Technology 2011. Warrendale, PA: The Minerals, Metals & Materials Society; 2011. p. 419-424.
29. Vojtech D, Kubasek J, Serak J, Novak P. Mechanical and corrosion properties of newly developed biodegradable Zn-based alloys for bone fixation. Acta Biomater. 2011; 7:3515–3522. [PubMed: 21621017]
30. Pospisilova, I.; Vojtech, D. Mechanical properties of Zn-Mg alloys. METAL 2013; Brno, Czech Republic. May 15–17, 2013; Slezska Ostrava, Czech Republic: Tanger; 2013.
31. Trumbo, P.; Yates, AA.; Schlicker, S.; Poos, M. Dietary Reference Intakes: Vitamin a, Vitamin K, Arsenic, Boron, Chromium, Copper, Iodine, Iron, Manganese, Molybdenum, Nickel, Silicon, Vanadium, And Zinc. Vol. 101. Washington, DC: National Academies Press; 2001. p. 294-301.
32. Fosmire GJ. Zinc toxicity. Am. J. Clin. Nutr. 1990; 51:225–227. [PubMed: 2407097]
33. Greenberg SA, Briemberg HR. A neurological and hematological syndrome associated with zinc excess and copper deficiency. J. Neurol. 2004; 251:111–114. [PubMed: 14999501]
34. Stefanidou M, Maravelias C, Dona A, Spiliopoulou C. Zinc: a multipurpose trace element. Arch. Toxicol. 2006; 80:1–9. [PubMed: 16187101]
35. Plum LM, Rink L, Haase H. The essential toxin: impact of zinc on human health. Int. J. Environ. Res. Public Health. 2010; 7:1342–1365. [PubMed: 20617034]
36. Nriagu, JO. Zinc toxicity in humans. In: Nriagu, JO., editor. Encyclopedia of Environmental Health. Burlington, NC: Elsevier; 2011. p. 801-807.
37. Murni NS, Dambatta MS, Yeap SK, Froemming GRA, Hermawan H. Cytotoxicity evaluation of biodegradable Zn–3Mg alloy toward normal human osteoblast cells. Mater. Sci. Eng., C. 2015; 49:560–566.
38. Williams DF. There is no such thing as a biocompatible material. Biomaterials. 2014; 35:10009–10014. [PubMed: 25263686]
39. Schaffer JE, Nauman EA, Stanciu LA. Cold drawn bioabsorbable ferrous and ferrous composite wires: An evaluation of in vitro vascular cytocompatibility. Acta Biomater. 2013; 9:8574–8584. [PubMed: 22885027]
40. Krezel A, Maret W. Zinc-buffering capacity of a eukaryotic cell at physiological pZn. JBIC, J. Biol. Inorg. Chem. 2006; 11:1049–1062. [PubMed: 16924557]
41. Ma JUN, Zhao N, Zhu D. Endothelial cellular responses to biodegradable metal zinc. ACS Biomater. Sci. Eng. 2015; 1:1174–1182. [PubMed: 27689136]
42. Bowen PK, Guillory R II, Shearier ER, Seitz JM, Drelich J, Bocks ML, et al. Metallic zinc exhibits optimal biocompatibilitiy for bioabsorbable endovascular stents. Mater. Sci. Eng., C. 2015; 56:467–472.
43. Black, J. Biological Performance of Materials: Fundamentals of Biocompatibility. 3rd. New York: Marcel Dekker; 1999.
44. Pourbaix, M. Atlas of Electrochemical Equilibria in Aqueous Solutions. Houston, TX: NACE; 1974.
45. Schneider CA, Rasband WS, Eliceiri KW. NIH Image to ImageJ: 25 years of image analysis. Nat. Methods. 2012; 9:671–675. [PubMed: 22930834]
46. Beers, Y. Introduction to the Theory of Error. 2nd. Reading, MA: Addison-Wesley; 1957.
47. Minitab 17 Statistical Software. State College, PA: Minitab, Inc.; 2010. www.minitab.com
48. Xiwei L, Sun J, Yang Y, Pu Z, Zheng Y. In vitro investigation of ultra-pure Zn and its mini-tube as potential bioabsorbable stent material. Mater. Lett. 2015; 161:53–56.
49. Rogers C, Tseng DY, Squire JC, Edelman ER. Balloon-artery interactions during stent placement. Circ. Res. 1999; 84:378–383. [PubMed: 10066671]
50. Cheneau E, John MC, Fournadjiev J, Chan RC, Kim H-S, Leborgne L, et al. Time course of stent endothelialization after intravascular radiation therapy in rabbit iliac arteries. Circulation. 2003; 107:2153–2158. [PubMed: 12695306]
51. Curcio A, Torella D, Indolfi C. Mechanisms of Smooth Muscle Cell Proliferation and Endothelial Regeneration After Vascular Injury and Stenting. Circ. J. 2011; 75:1287–1296. [PubMed: 21532177]

52. Hacker G. The morphology of apoptosis. Cell Tissue Res. 2000; 301:5–17. [PubMed: 10928277]
53. Maret W. Cellular zinc and redox states converge in the metallothionein/thionein pair. J. Nutr. 2003; 133:S1460–S1462.
54. Zhang K, Chen J. The regulation of integrin functions by divalent cations. Cell Adh and Mig. 2012; 6:20–29.
55. Dransfield I, Cabanas C, Craig A, Hogg N. Divalent cation regulation of the function of the leukocyto integrin LFA-1. J. Cell Biol. 1992; 116:219–226. [PubMed: 1346139]
56. Smith JW, Piotrowicz RS, Mathis D. A mechanism for divalent cation regulation of beta 3-integrins. J. Biol. Chem. 1994; 269:960–967. [PubMed: 7507113]
57. Qu A, Leahy DJ. The role of the divalent cation in the structure of the I domain form the CD11a/CD18 integrin. Structure. 1996; 4:931–942. [PubMed: 8805579]
58. Lymburner S, McLeod S, Purtzki M, Roskelley C, Xu Z. Zinc inhibits magnesium-dependent migration of human breast cancer MDA-MB-231 cells on fribronectin. J. Nutr. Biochem. 2013; 24:1034–1040. [PubMed: 23026493]
59. Thamilselvan V, Fomby M, Walsh M, Basson MD. Divalent cations modulate human colon cancer cell adhesion. J. Surg. Res. 2003; 110:255–265. [PubMed: 12697409]
60. Rink L, Gabriel P. Extracellular and immunological actions of zinc. BioMetals. 2001; 14:367–383. [PubMed: 11831466]
61. Chavakis T, May AE, Preissner KT, Kanse SM. Molecular mechanisms of zinc-dependent leukocyte adhesion involving the urokinase receptor and β_2-integrins. Blood. 1999; 93:2976–2983. [PubMed: 10216093]
62. Dorst K, Rammelkamp D, Hadjiargyrou M, Gersappe D, Meng Y. The effect of exogenous zinc concentration on the responsiveness of MC3T3-E1 Pre-osteoblasts to surface microtopography: part I (migration). Materials. 2013; 6:5517–5532.

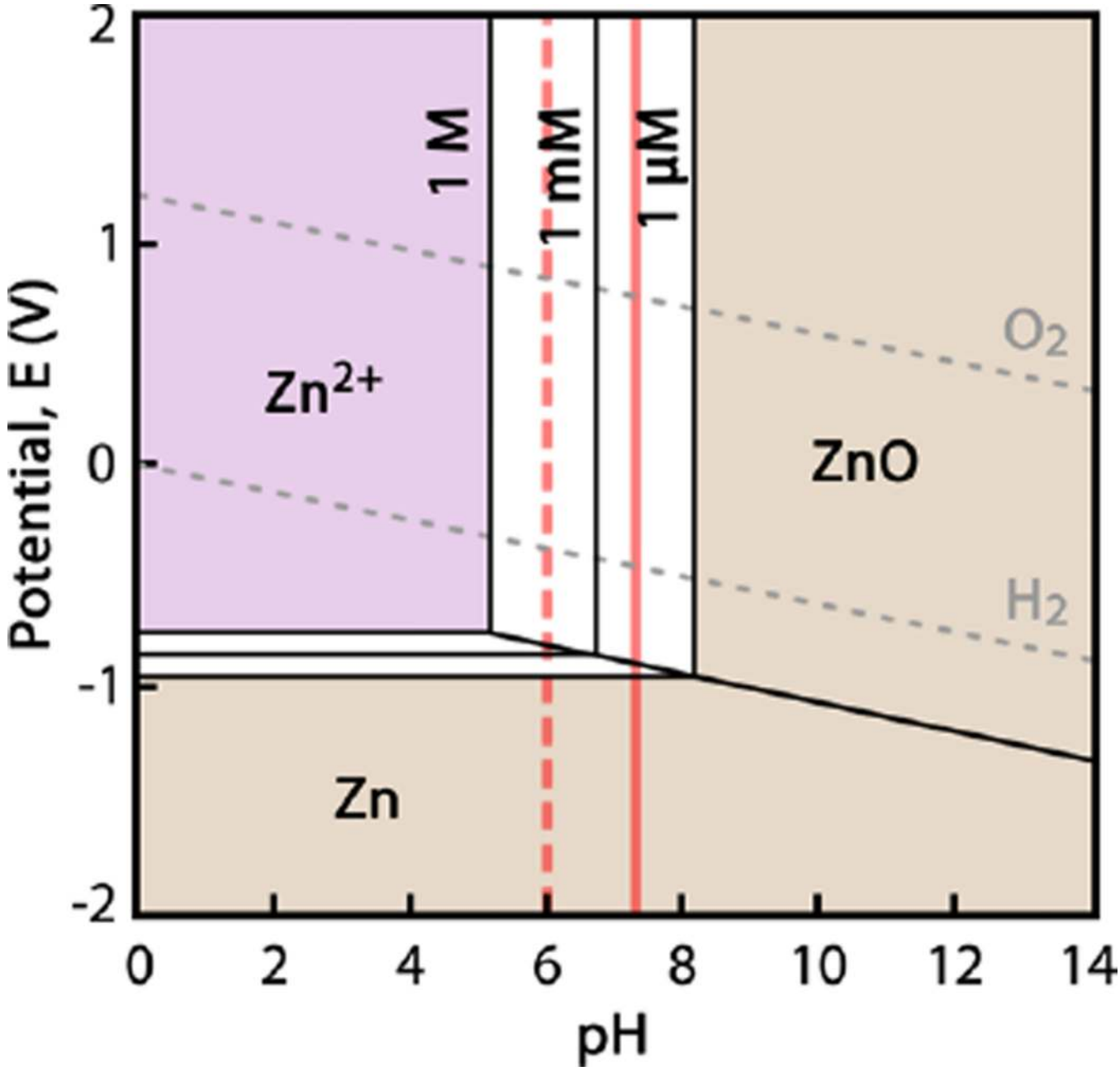

Figure 1.

Pourbaix diagram for Zn in water. Aqueous species have a light purple background, concentration-dependent regions between $[Zn^{2+}]$ = 1 μM and 1 M are white, and solid species are shown with orange backgrounds. Physiological pH 7.3 is shown by a solid red line, and pH 6 is shown by a broken red line. Calculated with FactSage software.

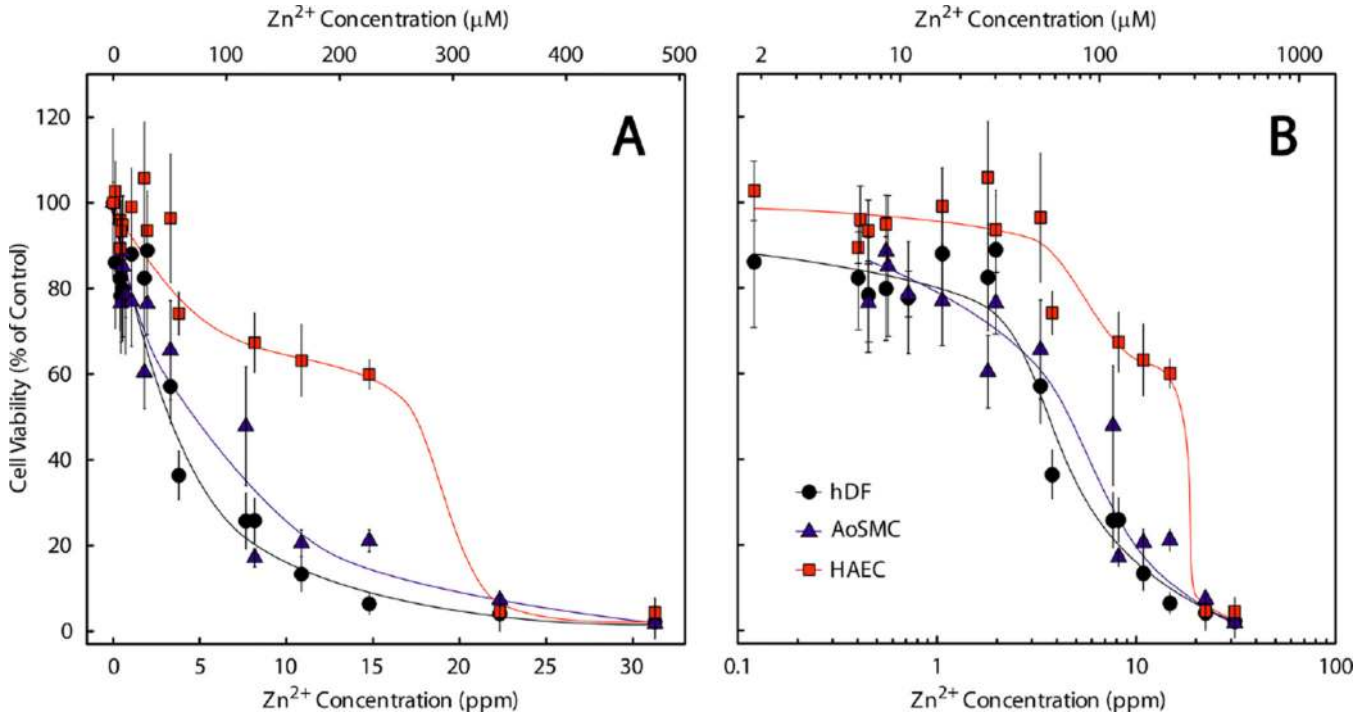

Figure 2.

Viability of hDF (●), AoSMC (▲), and HAEC (■) after being insulted with of Zn^{2+} in a pseudophysiological chloride solution carrier at pH 6. The data are shown in both linear (A) and log10 (B) scale.

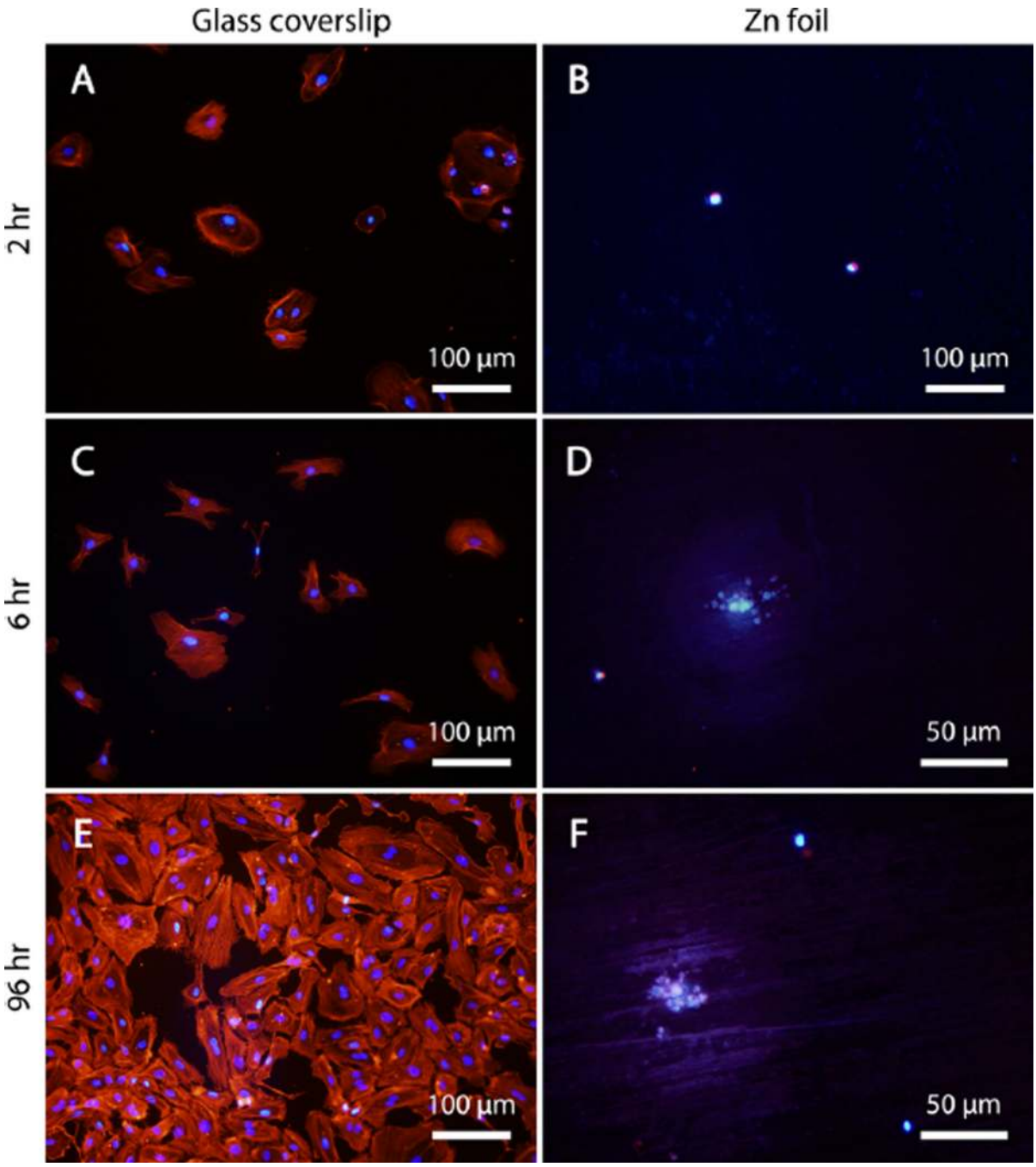

Figure 3.

Fluorescent imaging of early attachment of HAEC at (A, B) 2 and (C, D) 6 h, as well as long-term behavior at (E, F) 96 h. (A, C, E) A glass coverslip was used as a control surface conducive to cell growth, with which the cells' undesirable behavior on (B, D, F)the metallic zinc surface was compared. Note the difference in magnification in D and F compared to the other images.

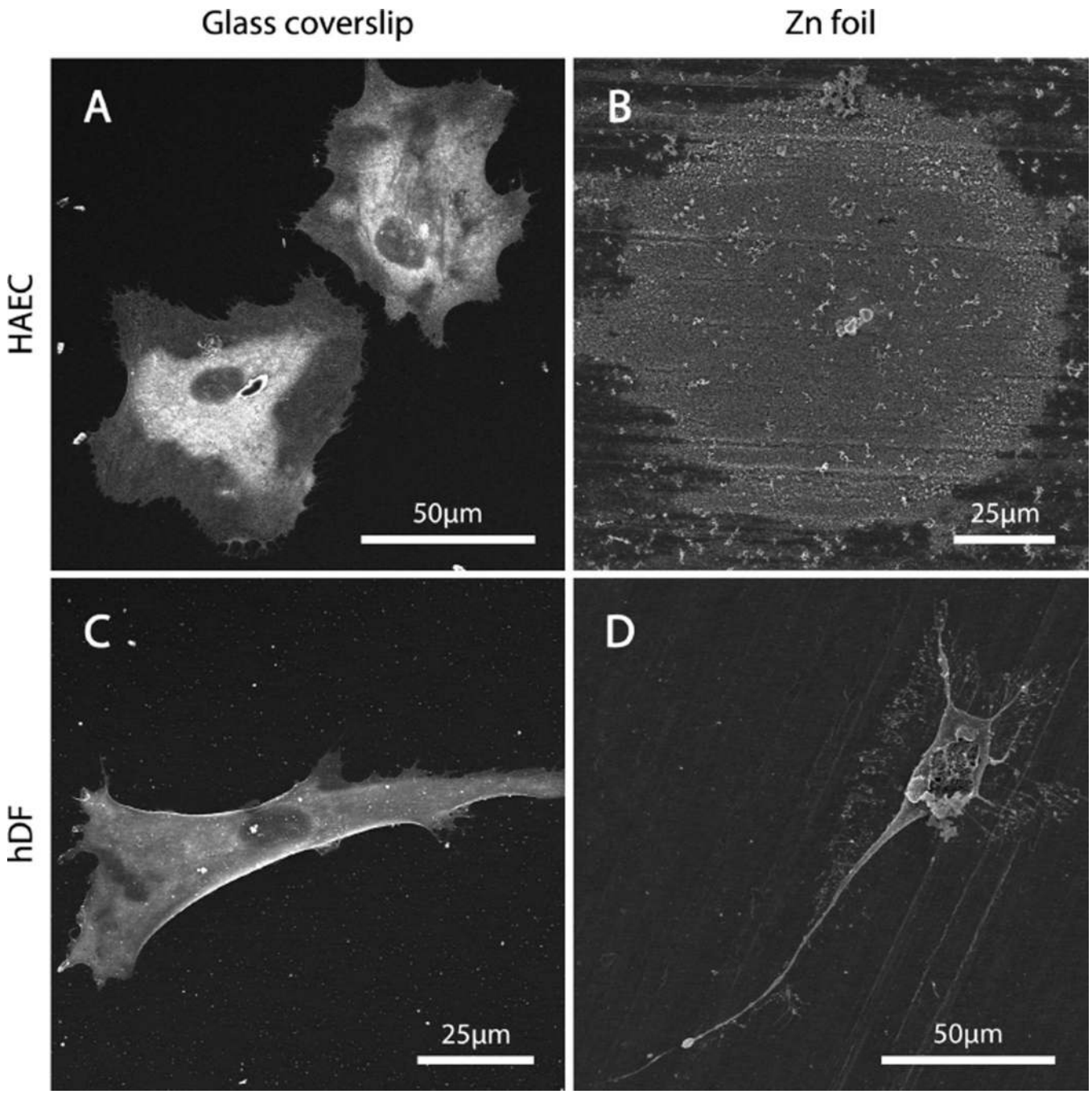

Figure 4.

Contrasting morphologies of (A, B) HAEC and (C, D) hDF cells cultured (A, C) on a glass coverslip stand in stark contrast to the cellular remains on (B, D) a metallic zinc foil after a 24 h culture period.

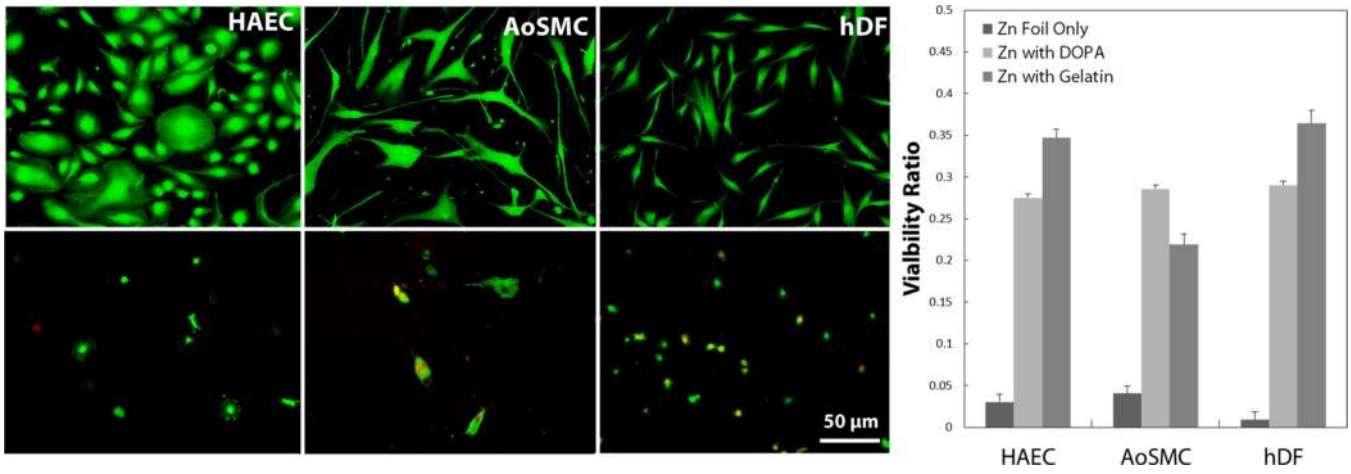

Figure 5.

Live/dead fluorescent imaging and quantification of cells cultured on control surface (top) and Zn surface modified with a layer of gelatin (bottom) after 24 h culture. Cell morphology was affected, leading to a more rounded phenotype. Cell viability ratios are significantly increased after surface modification compared to bare Zn surface.

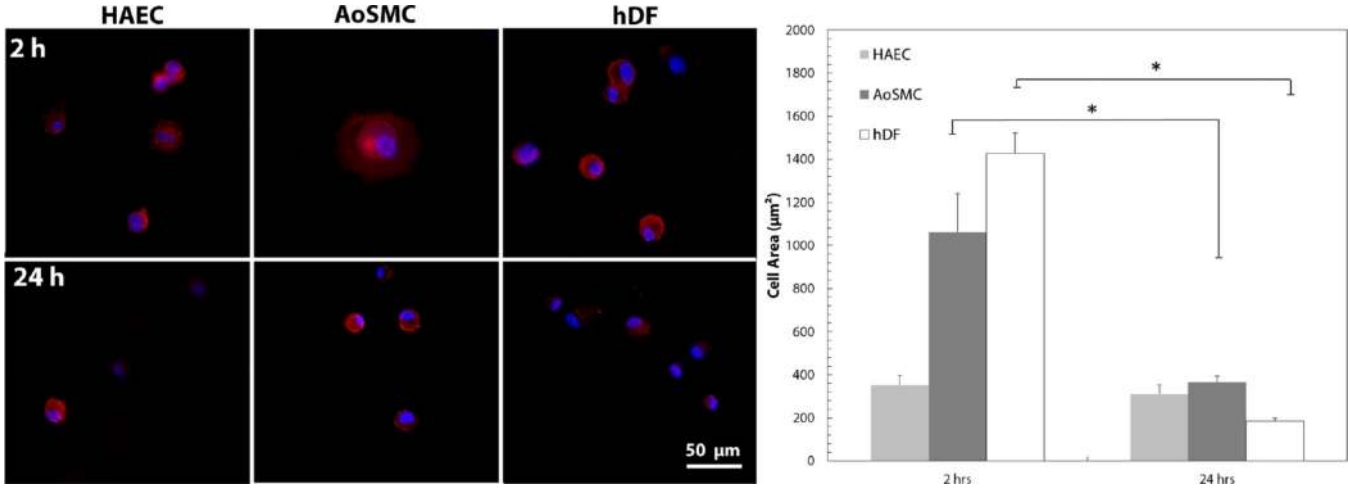

Figure 6.

Quantification of cell area after 2 and 24 h culture on modified Zn surface using F-actin and DAPI to visualize cells. Cell area was significantly decreased in AoSMC and hDF, but was not significantly changed in HAEC. * $p < 0.01$.

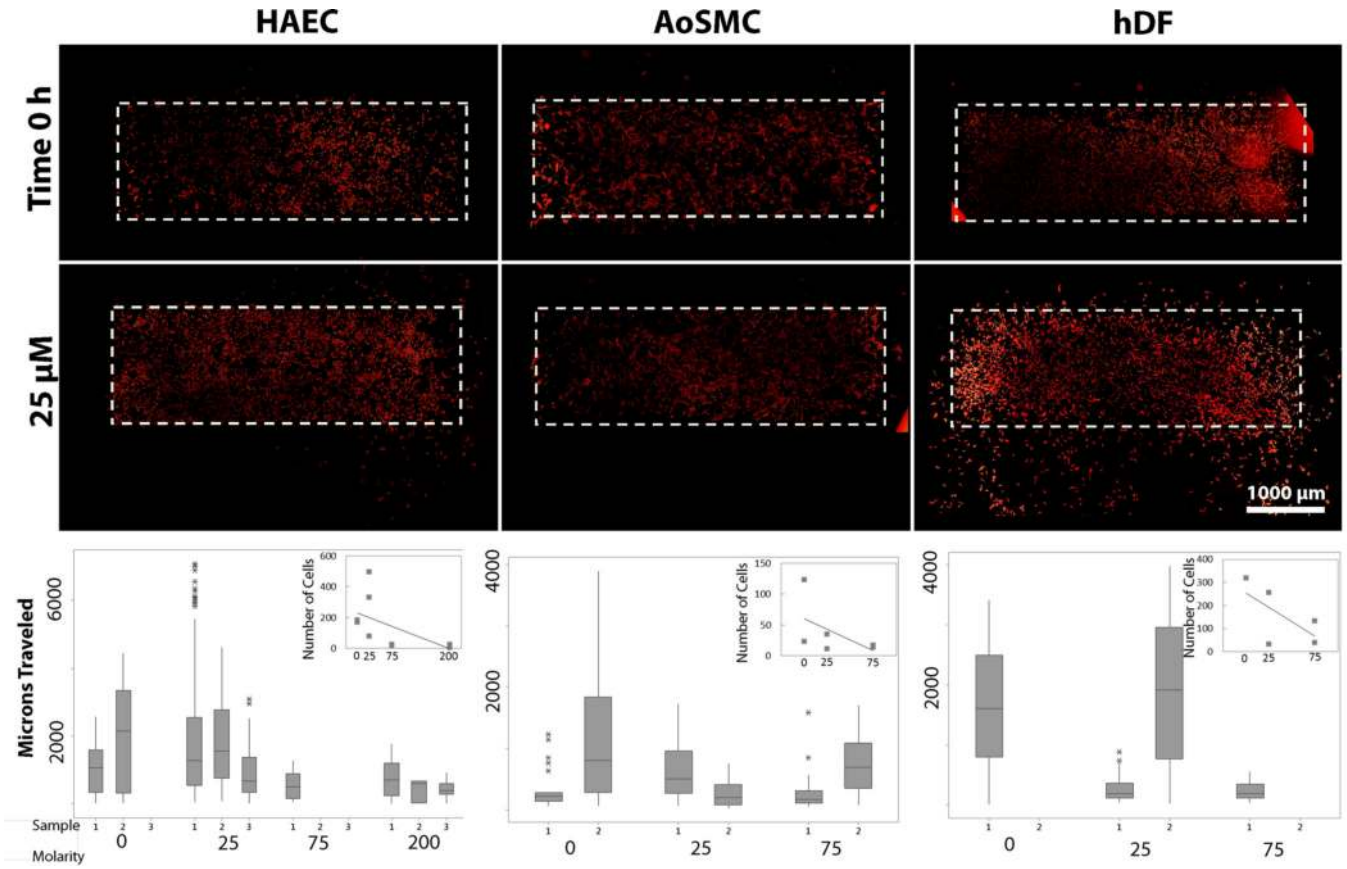

Figure 7.

Migration of vascular cell types under sublethal dose levels of Zn after 24 h exposure. Initial seeding area is indicated with a dashed white line and cells are visualized using F-actin. Number of cells migrating out of the initial area decreases with increasing Zn levels for all cell types.